Analysis of conduction and radiation heat transfer in a differentially heated 2-D square enclosure

Aritra Sasmal[1] and Subhash C. Mishra[2]
Department of Mechanical Engineering, IIT Guwahati, Guwahati – 781039, India

Author Manuscript

Abstract

Radiative heat transfer with and without conduction in a differentially heated 2-D square enclosure is analyzed. The enclosure with diffuse gray boundaries contains radiating and/or conducting gray homogeneous medium. Radiatively, the medium is absorbing, emitting and scattering. On the south boundary, four types of discrete heated regions, viz., the full boundary, the left one-third, left two third and middle one third, are considered. In the absence of conduction, distributions of heat flux along the south boundary are studied for the effect of extinction coefficient. In the presence of conduction, distributions of radiation, conduction and total heat fluxes along the south boundary are analyzed for the effects of extinction coefficient, scattering albedo, conduction-radiation parameter and south boundary emissivity. Effects of these parameters on centerline temperature distribution are also studied. To assess the performance of three commonly used radiative transfer methods, in all cases, the radiative transfer equation is solved using the discrete ordinate method (DOM), the conventional discrete ordinate method (CDOM) and the finite volume method (FVM). In the combined mode problem, with volumetric radiative information known from one of the three methods, viz., DOM, CDOM and FVM, the energy equation is solved using the finite difference method (FDM). In all cases, the results from FDM-DOM, FDM-CDOM and FDM-FVM are in good agreement. Computationally, all three sets of methods are equally efficient.

Keywords: Radiation, Conduction, Participating medium, Discrete ordinate method, Finite volume method

Nomenclature

A - area $\left(\mathrm{m}^2\right)$

[1] Contributed to this work during his stay in his BTech program at IIT Guwahati. Currently, graduate student, Dept. of Mechanical Engineering, University of Michigan, Ann Arbor, USA

[2] Corresponding author: Email: scm_iitg@yahoo.com, Tel: +91-361-2582660, Fax: +91-361-2690762.

This is the author manuscript accepted for publication and has undergone full peer review but has not been through the copyediting, typesetting, pagination and proofreading process, which may lead to differences between this version and the Version of Record. Please cite this article as doi: 10.1002/htj.21221.

This article is protected by copyright. All rights reserved.

c_p - specific heat $\left(\mathrm{J \cdot kg^{-1} \cdot K^{-1}}\right)$

G - incident radiation $\left(\mathrm{W \cdot m^{-2}}\right)$

I - intensity $\left(\mathrm{W \cdot m^{-2}}\right)$

$\hat{i}, \hat{j}, \hat{k}$ - unit vectors in x-, y-, z-directions, respectively (-)

k - thermal conductivity $\left(\mathrm{W \cdot m^{-1} \cdot K^{-1}}\right)$

M_θ, M_ϕ - number of discrete θ directions and ϕ directions (-)

m - index for direction (-)

N - conduction-radiation parameter, $\dfrac{k}{\left(4\sigma T_{\mathrm{ref}}^3\right)L}$ (-)

$\hat{n}$ - outward normal (-)

N_x, N_y - divisions of control volumes in x- and y-coordinate directions (-)

q - heat flux $\left(\mathrm{W \cdot m^{-2}}\right)$

S - source term $\left(\mathrm{W \cdot m^{-2}}\right)$

s - geometric distance in the direction of the intensity (-)

T - temperature $\left(\mathrm{K}\right)$

t - time $\left(\mathrm{s}\right)$

V - volume of the cell $\left(\mathrm{m^{-3}}\right)$

X, Y - dimensions of the 2-D rectangular enclosure $\left(\mathrm{m}\right)$

x, y, z - Cartesian coordinate directions (-)

Greek Symbols

α - thermal diffusivity $\left(\mathrm{m^2 \cdot s^{-1}}\right)$

β - extinction coefficient $\left(=\kappa_a + \sigma_s\right)$

θ - polar angle $\left(\mathrm{rad}\right)$

ϕ - azimuthal angle $\left(\mathrm{rad}\right)$

ε - emissivity (-)

κ_a - absorption coefficient $\left(\mathrm{m^{-1}}\right)$

ζ - dimensionless time, $\dfrac{\alpha t}{L^2}$ (-)

ρ - density $\left(\mathrm{kg \cdot m^{-3}}\right)$

μ - direction cosine with respect to the *x*-axis (-)

θ - dimensionless temperature (-)

η - direction cosine with respect to the y-axis (-)

This article is protected by copyright. All rights reserved.

Author Manuscript

σ - Stefan-Boltzmann constant = $5.67\times10^{-8}\,\mathrm{W/m^2\cdot K^4}$

σ_s - scattering coefficient $\left(\mathrm{m}^{-1}\right)$

Φ - emissive power (-)

Ω - direction, (θ,ϕ) (-)

$\Delta\Omega$ - solid angle, $\sin\theta d\theta d\phi$ (sr)

ω - scattering albedo $\left(=\frac{\sigma_s}{\beta}\right)$ (-)

Ψ - heat flux $\left(\mathrm{W\cdot m^{-2}}\right)$

Subscripts

b - boundary

C - conductive

E,W,N,S - east, west, north, south

P - cell center

R - radiative

ref - reference

T - total

x,y - for x-, y-faces of the control volume

Superscripts

m - index for the discrete direction

$*$ - non-dimensional quantity

1. Introduction

Consideration of thermal radiation with and without conduction is important in the analysis and design of a wide range of thermal systems [1-14]. If its consideration is paramount in the design and operation of high temperature thermal systems like boilers and furnaces [1, 13], it plays an important role in the thermal analysis of phase change processes of semitransparent materials, such as glass and silicon [8]. Heat transfer in porous insulations in the space shuttle is mainly by conduction and radiation [4,5]. Thermal radiation is a dominant mode of heat transfer in devices based on porous media combustion [6, 7]. These days, it has found applications in the diagnosis of tumors in the human body, and various types of laser based surgeries [9-11].

Unlike conduction and convection, apart from its dependence on spatial dimensions, thermal radiation depends on three extra variables, viz., polar angle, azimuthal angle and wavelength. For its dependence on polar and azimuthal angles, the governing radiative transfer equation (RTE) turns out to be an integro-differential one [12]. Except for a simple geometry, boundary conditions and medium condition, analytic solution of the RTE is seldom found [12]. Solution of the energy equations of combined mode heat transfer problems mostly rely on numerical methods like the finite difference method (FDM), the finite volume method (FVM), the finite element method (FEM),

Author Manuscript

This article is protected by copyright. All rights reserved.

the lattice Boltzmann method (LBM), etc. Even for the simple geometry, like a planar medium, analytic methods for the calculation of volumetric radiative information needed in the energy equation of the combined mode problems are expensive, and hence are hardly used. Thus, numerical methods for the solution of RTE that yield the needed volumetric radiative information are usually preferred.

Since 1950s, over a dozen numerical methods have been developed to solve the RTE [12]. In the absence of experimental results, if results from the Monte Carlo method are considered benchmark [12], statistical nature of its solution combined with its appetite for computational time, makes it incompatible with the solvers for the energy equations of combined mode problems [12]. Many physicists use P-N approximation [12, 15, 15]. The P-1 approximation provides accurate results for low optical thicknesses, and mathematical formulation, and solution of P-3 and higher order approximations are complex [12]. With other methods available, P-N approximation is not much preferred.

The discrete ordinate method (DOM) proposed by Chandrasekhar [17] in 1960s for stellar applications, was applied to engineering problems in 1980s by Fiveland [18], Truelove [19] and others [20-23]. Over the years, many researchers have preferred the DOM for its simple formulation and compatibility with solvers of the combined mode problems [24]. Ray effect and false scattering have been reported as its drawback [25, 26]. To address the drawback of the DOM, in 1980s, Shah proposed the discrete transfer method [27]. This method has been applied to a wide range of problems [28, 29]. However, in multi-dimensional geometry, in the combined mode problems, its implementation is difficult, and solution is computationally expensive.

Encouraged by the applications of the finite volume method (FVM) to fluid flow and heat transfer problems, Raithby and Chui [30], Chai and Patankar [31], Murthy and Mathur [32] extended its application to the solution of radiative heat transfer problems. For its flexible spatial and angular computation grids, the FVM has been applied to a wide range of problems [33-36]. Though the spatial computational grid of the DOM [12, 18, 19] is flexible like the FVM, its angular grid is not. In the DOM [12, 18, 19], in the calculation of radiative information, the discrete directions in the $4\pi-$ spherical space are predefined by the approximation used. Ordinates and the associated weights for calculation of incident radiation and radiative heat flux are obtained from the tabulated data [12]. In the FVM, however, depending upon the need, one has the freedom to discretize the angular space, and the associated weights are calculated with a simple formula [30-36].

In 2006, Mishra et al. [37] revisited the DOM [18, 19] and the FVM [30-32]. It was found that in both the DOM and the FVM, the RTE is resolved along the coordinate directions. In the FVM, the angular weight is calculated by integrating the corresponding direction cosine over the discrete solid angle, while in the DOM, no such integration is done. Spatial integration of the RTE and ray marching procedures in both DOM and FVM are the same. With the objective of making the DOM as flexible as the FVM, Mishra et al. [37] relaxed the constraint on angular discretization and calculation of the associated weights. The modified DOM (MDOM) that has a close resemblance with the DOM and the FVM has been found to provide accurate results in a wide range of problems in planar, cylindrical and spherical geometry [38-41].

This article is protected by copyright. All rights reserved.

Author Manuscript

In assessing the performance of any method, normally the chosen geometry has homogeneous boundary conditions. However, the versatility of a numerical radiative transfer method is better assessed with discontinuous boundary conditions. The present work focuses on this aspect. With two variants of the DOM and the FVM, accuracies of the methods in solving two types of problems in a 2-D square enclosure are assessed. With different regions of the south boundary as the radiation source (heated region), this problem deals with only the radiation aspect, and belongs to the class of radiative equilibrium. The second problem pertains to the solution of the combined mode conduction and radiation heat transfer with similar discrete heating regions on the south boundary. For the sake of comparison of the three methods, the DOM with predefined ordinates and weights [12] is termed as conventional DOM (CDOM), while the MDOM [37] is referred to as the DOM. In the case of the radiation equilibrium problem, effect of the extinction coefficient on heat flux distributions on the south boundary and centerline temperature profiles are compared. In the case of combined mode conduction and radiation heat transfer, for four heated regions, effects of extinction coefficient, scattering albedo, conduction-radiation parameter and emissivity on the steady-state (SS) conduction heat flux, radiation heat flux and total heat flux along the south boundary are compared and analyzed. With the same parameters, in all cases, the centerline temperature distributions are also compared and analyzed.

2. Formulation

Consideration is given to a 2-D square enclosure (Figure 1a) with diffuse-gray boundaries containing radiating and conducting homogeneous gray medium. Radiatively, the medium is absorbing, emitting and scattering. In radiative equilibrium, depending upon the cases, either full or part of the south boundary is the radiation source, and the medium temperature is unknown. In the combined mode conduction and radiation heat transfer problem, initially, the entire system is at temperature T_0 and for time $t > 0$, all or part of the south boundary is maintained at a higher temperature. With thermophysical properties such as the density ρ, the specific heat c_p and the thermal conductivity k constant, the energy equation for the combined mode problem can be written as

$$\rho c_p \frac{\partial T}{\partial t} = k\left(\frac{\partial^2 T}{\partial x^2} + \frac{\partial^2 T}{\partial y^2}\right) - \nabla \cdot q_R \tag{1}$$

where in Eq. (1), the volumetric radiative source term $\nabla \cdot q_R$ is given by

$$\nabla \cdot q_R = \kappa_a \left(4\pi I_b - G\right) \tag{2}$$

where κ_a is the absorption coefficient, $I_b = \frac{\sigma T^4}{\pi}$ is the Planck blackbody intensity and G is the incident radiation. With I as the intensity of radiation, $\theta\left(0 \le \theta \le \pi\right)$ as the polar angle and $\phi\left(0 \le \phi \le 2\pi\right)$ as the azimuthal angle (Fig. 1b), G is given by and computed from the following

This article is protected by copyright. All rights reserved.

$$G = \int_{\phi=0}^{2\pi} \int_{\theta=0}^{\pi} I(\theta,\phi)\sin\theta d\theta d\phi \approx \sum_{m=1}^{M_\theta \times M_\phi} I^m w_g^m \tag{3}$$

In Eq. (3), M_θ and M_ϕ are the numbers of discrete divisions of the polar $\theta\left(0 \le \theta \le \pi\right)$ and the azimuthal $\phi\left(0 \le \phi \le 2\pi\right)$ angles, respectively, $M_\theta \times M_\phi$ is the total number of discrete directions considered in the $4\pi-$spherical space, and m is the index for the discrete direction. In Eq. (3), w_g^m is the weight associated with intensity I^m in the direction having index m. The discrete intensity I^m is obtained from the solution of the RTE given by

$$\frac{dI^m}{ds^m} = -\beta I^m + S^m \tag{4}$$

where with reference to Fig. 1b, s^m is the distance in the direction $\hat{s}^m = \left(\sin\theta^m \cos\phi^m\right)\hat{i} + \left(\sin\theta^m \sin\phi^m\right)\hat{j} + \left(\cos\theta^m\right)\hat{k}$, β is the extinction coefficient and S^m is the source term given by

$$S^m = \beta\left(1-\omega\right)\left(\frac{\sigma T^4}{\pi}\right) + \frac{\beta\omega}{4\pi} G \tag{5}$$

where ω is the scattering albedo. In all three methods (DOM, CDOM, FVM) considered, next Eq. (4) is resolved along the coordinate directions. For the 2-D rectangular enclosure considered, in the present work, Eq. (4) is written as

$$\mu^m \frac{\partial I^m}{\partial x} + \xi^m \frac{\partial I^m}{\partial y} = -\beta I^m + S^m \tag{6}$$

where μ^m and ξ^m are the x- and y-direction cosines, respectively. Integration of Eq. (6) over the elemental control volume $\Delta V = \Delta x \times \Delta y \times 1$ leads to

$$\mu^m \left(I_E^m - I_W^m\right)\Delta y + \xi^m \left(I_N^m - I_S^m\right)\Delta x = -\beta I_P^m + S_P^m \tag{7}$$

where in Eq. (7), with reference to Fig. 1a, in the direction having index m, I_E^m, I_W^m, I_N^m and I_S^m are the face averaged intensities located at the centers of the east, west, north and south faces, respectively. Here I_P^m and S_P^m are the volume averaged intensity and source term located at the cell center, respectively. For a diffuse gray boundary with emissivity ε_b and temperature T_b, boundary intensities known from Eq. (8), the solution of Eq. (7) starts from each of the four corners (quadrants). For example, when the computation starts from the south-west corner (quadrant 1), the known intensities are I_S^m and I_W^m. Similarly, while marching from the south-east (quadrant 2),

Author Manuscript

This article is protected by copyright. All rights reserved.

north-east (quadrant 3) and north-west (quadrant 4), in Eq. (7), the known intensities are $\left(I_S^m, I_E^m\right)$, $\left(I_N^m, I_E^m\right)$ and $\left(I_N^m, I_W^m\right)$, respectively.

$$I_b = \frac{\varepsilon_b \sigma T_b^4}{\pi} + \left(\frac{1-\varepsilon_b}{\pi}\right) \int_{\hat{n}\cdot\hat{s}<0} I(\Omega)\left|\hat{n}\cdot\hat{s}\right| d\Omega \tag{8}$$

While marching from every quadrant (Fig. 1a), from Eq. (7), intensities are calculated at the cell center P. To reduce the number of unknown intensities, the diamond scheme (Eq. (9)) is invoked to related face-center and cell-center intensities.

$$I_P^m = \frac{I_E^m + I_W^m}{2} = \frac{I_S^m + I_N^m}{2} \tag{9}$$

For marching from the 4 corners, this leads to

$$I_P^m = \frac{2\mu^m A_x I_W^m + 2\xi^m A_y I_S^m + \left(V\Delta\Omega^m\right) S_P^m}{2\mu^m A_x + 2\xi^m A_y + \beta V \Delta\Omega^m}, \text{1st quadrant: } \mu^m > 0,\ \xi^m > 0 \tag{10a}$$

$$I_P^m = \frac{2\left|\mu^m\right| A_x I_E^m + 2\xi^m A_y I_N^m + \left(V\Delta\Omega^m\right) S_P^m}{2\left|\mu^m\right| A_x + 2\xi^m A_y + \beta V \Delta\Omega^m}, \text{2nd quadrant: } \mu^m < 0,\ \xi^m > 0 \tag{10b}$$

$$I_P^m = \frac{2\left|\mu^m\right| A_x I_E^m + 2\left|\xi^m\right| A_y I_N^m + \left(V\Delta\Omega^m\right) S_P^m}{2\left|\mu^m\right| A_x + 2\left|\xi^m\right| A_y + \beta V \Delta\Omega^m}, \text{3rd quadrant: } \mu^m < 0,\ \xi^m < 0 \tag{10c}$$

$$I_P^m = \frac{2\mu^m A_x I_W^m + 2\left|\xi^m\right| A_y I_N^m + \left(V\Delta\Omega^m\right) S_P^m}{2\mu^m A_x + 2\left|\xi^m\right| A_y + \beta V \Delta\Omega^m}, \text{4th quadrant: } \mu^m > 0,\ \xi^m < 0 \tag{10d}$$

With I_P^m known, from Eq. (9), the two unknown face-center intensities are calculated. In spatial marching, for the next control volume, these two intensities are known in Eq. (10). With indices (i, j) for $\left(1 \le i \le N_x, 1 \le j \le N_y\right)$ where $N_x \times N_y$ are the number of control volumes, for example, while marching from quadrant 1, for the south boundary control volumes $(i,1)$, the east face intensities $I_{E,(i,1)}^m$ for $(i,1)^{\text{th}}$ control volume becomes the west face intensities $I_{W,(i+1,1)}^m$ for the $(i+1,1)^{\text{th}}$ control volume, i.e., $I_{W,(i+1,1)}^m = I_{E,(i,1)}^m$. Similarly, in the north-south direction, $I_{S,(i,2)}^m = I_{N,(i,1)}^m$. It is to be noted that in the expressions of I_P^m (Eqs. (10a-d)), the source term S_P^m (Eq. (5)) is a function of intensity. Thus, to facilitate the computation of I_P^m, in the iterative

This article is protected by copyright. All rights reserved.

procedure, S_P^m is taken from the previous iteration, and in the first iteration, some guess value is taken.

The formulation and procedure outlined above remain common to the three methods, viz., FVM, CDOM and DOM considered in the present work, except in the FVM, in Eqs. (10a-d), the direction cosines μ^m and ξ^m, are modified to the angular weights D_x^m and D_y^m, respectively.

$$D_x^m = \int_{\phi^m-\frac{\Delta\phi}{2}}^{\phi^m+\frac{\Delta\phi}{2}} \int_{\theta^m-\frac{\Delta\theta}{2}}^{\theta^m+\frac{\Delta\theta}{2}} (\sin\theta\cos\phi)\sin\theta d\theta\, d\phi$$
$$= \cos\phi^m \sin\left(\frac{\Delta\phi}{2}\right)\left[\Delta\theta - \cos(2\theta^m)\sin(\Delta\theta)\right] \quad (11)$$

$$D_y^m = \int_{\phi^m-\frac{\Delta\phi}{2}}^{\phi^m+\frac{\Delta\phi}{2}} \int_{\theta^m-\frac{\Delta\theta}{2}}^{\theta^m+\frac{\Delta\theta}{2}} (\sin\theta\sin\phi)\sin\theta d\theta\, d\phi$$
$$= \sin\phi^m \sin\left(\frac{\Delta\phi}{2}\right)\left[\Delta\theta - \cos(2\theta^m)\sin(\Delta\theta)\right] \quad (12)$$

Further, the term $\Delta\Omega^m$ takes the form

$$\Delta\Omega^m = \int_{\phi^m-\frac{\Delta\phi}{2}}^{\phi^m+\frac{\Delta\phi}{2}} \int_{\theta^m-\frac{\Delta\theta}{2}}^{\theta^m+\frac{\Delta\theta}{2}} \sin\theta d\theta\, d\phi = 2\sin\theta^m \sin\left(\frac{\Delta\theta}{2}\right)\Delta\phi \quad (13)$$

In the CDOM and DOM, $\Delta\Omega^m = 1.0$. With intensity distributions at the face centers and cell centers known from the above, in all three methods, viz., FVM, DOM and CDOM, the radiative heat flux is calculated from the following:

$$q_R = \int_{\Omega=0}^{4\pi} I(\Omega)(\hat{s}\cdot\hat{n})\, d\Omega \quad (14)$$

where $\hat{n}$ is the outward normal to the surface. On the *y*-face (south and north boundaries) and the *x*-face (west and east boundaries), in FVM and DOM, the expressions of heat flux take the form

$$q_{R,x} = \sum_m^{M_\theta \times M_\phi} I^m D_x^m \quad (15)$$

$$q_{R,y} = \sum_m^{M_\theta \times M_\phi} I^m D_y^m \quad (16)$$

Author Manuscript

This article is protected by copyright. All rights reserved.

In the CDOM, the direction cosines μ^m and ξ^m needed in Eqs. (10a-d), and angular weight w^m for the discrete direction with index m is based on the pre-tabulated data reported in [12].

$$q_{R,x} = \sum_{m}^{M_\theta \times M_\phi} I^m \mu^m w^m \tag{17}$$

$$q_{R,y} = \sum_{m}^{M_\theta \times M_\phi} I^m \xi^m w^m \tag{18}$$

In the DOM and the FVM, there is flexibility in choosing the angular grid, and calculation of the associated weights can be customized according to the need, while the CDOM lacks this flexibility.

In the combined mode conduction-radiation problem, the solution of the energy equation (Eq. (1)) needs the volumetric radiative information given by Eq. (2). In Eq. (2), the incident radiation G is calculated from Eq. (3). In the calculation of G, in the FVM and the DOM, the weight $w_g^m = \Delta\Omega^m$ (Eq. (13)), while in the CDOM, $w_g^m = w^m$ is based on tabulated data [12].

For generality, the pertinent equations are written in non-dimensional form. With L as the reference length and T_R as the reference temperature, non-dimensional distance η, time ζ, temperature Θ, conduction-radiation parameter N, intensity I^*, radiative heat flux Ψ_R, conductive heat flux Ψ_c, and incident radiation G^* defined as

$$\eta_x = \frac{x}{L},\ \eta_y = \frac{y}{L},\ \zeta = \frac{\alpha t}{L^2},\ \Theta = \frac{T}{T_{\text{ref}}},\quad N = \frac{k}{\left(4\sigma T_{\text{ref}}^3\right)L}$$

$$I^* = \frac{I}{\left(\sigma T_{\text{ref}}^4/\pi\right)},\ \Psi_c = \left.\frac{\partial\Theta}{\partial\eta_y}\right|_{\eta_y=0}\quad \Psi_R = \frac{q_R}{\sigma T_{\text{ref}}^4},\ G^* = \frac{G}{\left(\sigma T_{\text{ref}}^4/\pi\right)} \tag{19}$$

Equations (1) and (2) take the form

$$\frac{\partial\Theta}{\partial\zeta} = \frac{\partial^2\Theta}{\partial\eta_x^2} + \frac{\partial^2\Theta}{\partial\eta_y^2} - \frac{1}{4N}\nabla\cdot\Psi_R \tag{20}$$

$$\nabla\cdot\Psi_R = \beta(1-\omega)\left(4\Theta^4 - \frac{G^*}{\pi}\right) \tag{21}$$

In the present work, in the combined mode conduction-radiation problem, the entire system is initially at known temperature $\Theta_0\left(=\frac{T_0}{T_R}\right)$, and for time $\zeta > 0$, either all or part of the south is

This article is protected by copyright. All rights reserved.

Author Manuscript

raised to temperature $\Theta_S \left(= \frac{T_S}{T_R} \right)$. With initial and boundary conditions known, Eq. (20) is solved using the alternate direction implicit scheme. The solution of Eq. (20) is iterative. At any time level, the radiative information $\nabla \cdot \Psi_R$ is obtained from the temperature field of the medium known from the previous iteration. In the first iteration, $\nabla \cdot \Psi_R$ is based on the initial temperature field.

3. Results and Discussion

Before analyzing results for various cases, results of grid- and ray-independency are presented first in Table 1. For a black square enclosure with the entire south boundary as the radiation source and non-isothermal medium, non-dimensional radiative heat flux Ψ_R at locations $\eta_x = 0.25$ and 0.50 on the south boundary are compared against the number of control volumes and rays. These results are shown for extinction coefficient $\beta = 1.0$. Results from the DTM [42] are taken as benchmark. For $M_\theta \times M_\phi = 6 \times 8$ rays, in all three methods, no noticeable change is found beyond 30×30 control volumes. Similarly, for $N_x \times N_y = 30 \times 30$ control volumes, $M_\theta \times M_\phi = 6 \times 8$ (S_6 in the CDOM) rays is found sufficient. In the following, thus all results are for $N_x \times N_y = 30 \times 30$ control volumes and $M_\theta \times M_\phi = 6 \times 8$ rays. In the combined mode conduction-radiation problem, the time step $\Delta\zeta = 10^{-3}$ was used, and steady-state was assumed to have been reached when temperature at all locations between two successive iterations was $\leq 10^{-5}$.

3.1 Enclosure under radiative equilibrium

In the absence of conduction, with medium temperature unknown, and a completely or partially heated south boundary as the radiation source, the problem under consideration reduces to radiative equilibrium. In this case, $\nabla \cdot \Psi_R = 0$. This amounts to $\omega = 1.0$ (Eq. (21)). For the extinction coefficient $\beta = 0.1, 1.0$ and 3.0, distributions of non-dimensional radiative heat flux Ψ_R along the south boundary are shown in Figs. 2a-e for heated regions $0.0 \leq \eta_x \leq 1.0$, $0.33 \leq \eta_x \leq 0.66$, $0 \leq \eta_x \leq 0.33$, $0 \leq \eta_x \leq 0.66$ and $\{0 \leq \eta_x \leq 0.33\} \cup \{0.66 \leq \eta_x \leq 1.0\}$, respectively. For a higher β, in the heated region, radiative heat flux Ψ_R is less. The trend is the same in the unheated region. In the heated region, the magnitude is less than that in the unheated reason. The net heat flux is the vector sum of the heat flux due to the outgoing diffuse intensities and the intensities incident on it from the medium. In the unheated region, only the intensities incident from the medium contributes to the radiative heat flux, hence it has a negative magnitude. With an increase in β, the contribution of radiation to the south boundary from the medium increases, and as a result, in the heated region the net heat flux decreases. Results from FVM, CDOM and DOM compare exceedingly well.

3.2 Combined mode conduction-radiation heat transfer

Author Manuscript

This article is protected by copyright. All rights reserved.

3.2.1 Heat flux distributions

In the combined mode conduction-radiation heat transfer problem, four different heated regions, viz., $0.0 \le \eta_x \le 1.0$, $0.33 \le \eta_x \le 0.66$, $0 \le \eta_x \le 0.33$, and $0 \le \eta_x \le 0.66$ on the south boundary are considered. With temperature of the heated region Θ_S, temperature of other regions of the south boundary and the other three boundaries are maintained at $\Theta_b = 0.1\Theta_S$. Effects of the extinction coefficient β, the scattering albedo ω, the conduction-radiation parameter N and the emissivity ε of the south boundary on distributions of steady-state conductive heat flux Ψ_C, radiative heat flux Ψ_R and total heat flux $\Psi_T \left(= \Psi_R + 4N\Psi_C\right)$ along the south boundary are analyzed. Effects of these parameters on centerline $\left(0.5, \eta_y\right)$ non-dimensional temperature Θ are also studied.

Effect of extinction coefficient

For the extinction coefficients $\beta = 0.1$, 1.0 and 5.0, for the four heated regions on the south boundary, distributions of Ψ_C, Ψ_R and Ψ_T are shown in Figs. 3-4. For heated region $0.0 \le \eta_x \le 1.0$, results are shown in Figs. 3a-c for $\beta = 0.1$, 1.0 and 5.0, respectively. Figures 3d-f, 4a-c and 4d-f show corresponding results for heated regions $0.33 \le \eta_x \le 0.66$, $0 \le \eta_x \le 0.33$, and $0 \le \eta_x \le 0.66$, respectively. With all boundaries black, these results are shown for $\omega = 0.5$ and $N = 0.1$.

An observation of Figs. 3 and 4 shows that with an increase in β, in the heated region, the conduction heat flux Ψ_C decreases marginally. However, the decrease is pronounced in the radiation heat flux Ψ_R, and accordingly, the total heat flux Ψ_T, also decreases significantly. The major contribution to the total heat flux Ψ_T in the heated region is from radiation. Contribution of radiation decreases with an increase in β, and accordingly Ψ_T decreases. It is observed that the greater the area of the heated region, the lower the total heat flux Ψ_T. This is because the radiation received by the medium that appears as the diffuse radiation decreases with a decrease in the area of the heated region. Thus, for a decrease in the area of the heated region, for a given β, any region (heated or unheated) of the south boundary receives less radiation from the medium. It is further observed that Ψ_C, Ψ_R and Ψ_T for the region $0.33 \le \eta_x \le 0.66$ (Figs. 3d-f) is less than that for the region $0 \le \eta_x \le 0.33$ (Figs. 4a-c). This is because for a given β, the heated region close to the side boundary (Figs. 4a-c) receives less radiation from the medium than the heated central region $0.33 \le \eta_x \le 0.66$ (Figs. 3d-f). An observation of Figs. 4-5 shows that results from all three methods compare exceedingly well.

Effect of scattering albedo

This article is protected by copyright. All rights reserved.

For $\beta = 1.0$ and $N = 0.1$, effects of the scattering albedo ω on distributions of Ψ_C, Ψ_R and Ψ_T along the south boundary for the heated regions $0.0 \le \eta_x \le 1.0$, $0.33 \le \eta_x \le 0.66$, $0 \le \eta_x \le 0.33$, and $0 \le \eta_x \le 0.66$ are shown in Figs. 5a-c, 5d-f, 6a-c and 6d-f, respectively. Figures 5a, 5d, 6a and 6d show results for $\omega = 0.0$, Figs. 5b, 5e, 6b and 6e for $\omega = 0.5$, and Figs. 5c, 5f, 6c and 6f for $\omega = 0.8$. Scattering increases with an increase in ω, and this strengthens the radiation from the medium close to the south boundary, and accordingly, the radiative heat flux in the heated region decreases and in the unheated region, its magnitude increases. Results from all three methods are in excellent agreement.

Effect of conduction-radiation parameter

Effect of the conduction-radiation parameter N on distributions of Ψ_C, Ψ_R and Ψ_T along the south boundary for the heated regions $0.0 \le \eta_x \le 1.0$, $0.33 \le \eta_x \le 0.66$, $0 \le \eta_x \le 0.33$, and $0 \le \eta_x \le 0.66$ are shown in Figs. 7a-c, 7d-f, 8a-c and 8d-f, respectively. Other parameters used for these results are $\beta = 1.0$ and $\omega = 0.0$. Figures 7a, 7d, 8a and 8d show the results for $N = 0.01$, Figs. 7b, 7e, 8b and 8e for $N = 0.1$, and Figs. 7c, 7f, 8c and 8f for $N = 1.0$. With other parameters fixed, radiation dominates over conduction when $N\left(\frac{O(\Psi_C)}{O(\Psi_R)}\right)$ decreases. For any heated region, this is what is observed from Figs. 7 and 8, i.e., the lower the value of N, the higher is the contribution of radiation to the total heat flux Ψ_T. For a particular heated region, with an increase in N, in the heated region, the magnitude of Ψ_R increases, which in turns increases the magnitude of Ψ_T. When N increases, the heated region receives less radiation from the medium, and this increases the net radiative heat flux Ψ_T. Also, because of the increased amount of radiation, in the unheated region, the magnitude of conduction heat flux is more.

Effect of south boundary emissivity

Figure 9 shows the effect of the emissivity of the south boundary on distributions of Ψ_C, Ψ_R and Ψ_T. In Figs. 9a-c and 9d-f, for emissivity $\varepsilon = 0.2$, 0.6 and 1.0, these distributions are shown for the heated regions $0.0 \le \eta_x \le 1.0$ and $0 \le \eta_x \le 0.33$, respectively. The other three boundaries are black. These results are shown for $\beta = 0.1, \omega = 0.5$ and $N = 0.1$. When emissivity ε increases, in the boundary intensity (Eq. (8)), the contribution of theemitted component goes up and the contribution of the reflected component goes down. As a result, the medium receives more radiation emitted from the boundary. This results in higher radiative heat flux as observed in Fig. 9. With an increase in ε of the south boundary, the medium in the vicinity of the boundary gets more heated, and hence the conduction heat flux decreases. For the chosen values of the parameters, the contribution of radiation to the total heat flux is much more than that of conduction, and hence the total heat flux increases. Results of all three methods are in good agreement.

This article is protected by copyright. All rights reserved.

Author Manuscript

3.2.2 Temperature distribution

Effects of the extinction coefficient β, the scattering albedo ω and the conduction-radiation parameter N on SS non-dimensional centerline $(0.5, \eta_y)$ temperature Θ are shown in Figs. 10 and 11. In Figs. 10a-c, 10d-f, 11a-c and 11d-f, these results are shown for the heated regions $0.0 \le \eta_x \le 1.0$, $0.33 \le \eta_x \le 0.66$, $0 \le \eta_x \le 0.33$, and $0 \le \eta_x \le 0.66$, respectively. For a particular heated region, while analyzing the effect of a parameter, say β, the other parameters (ω, N) are held constant and have the same values as that for the results on heat flux distributions considered in the previous section.

For heated region $0.0 \le \eta_x \le 1.0$, effects of β, ω and N on $\Theta(0.5, \eta_y)$ are shown in Figs. 10a-c, respectively. Similarly, effects of β, ω and N on $\Theta(0.5, \eta_y)$ for the heated regions $0.33 \le \eta_x \le 0.66$, $0 \le \eta_x \le 0.33$, and $0 \le \eta_x \le 0.66$ are shown in Figs. 10d-f, 11-a-c and 11d-f, respectively. A comparison of Figs. 10a, 10d, 11a and 11d shows that with an increase in β, temperature at any location becomes greater. When the extinction coefficient β increases, owing to enhanced extinction, the medium becomes more heated. The higher the area of the heated region,the higher the temperature $\Theta(0.5, \eta_y)$. It is to be noted that in Fig. 11a, $\Theta(0.5, \eta_y)$ profile is different from that of Figs. 10a, 10d and 11d. This is for the mere fact that in the case for the heated region $0 \le \eta_x \le 0.33$, the centerline $(0.5, \eta_y)$ passes through the cold region of the south boundary. In this case, as is observed, the effect of the heated region is felt some distance away from the south boundary.

Contrary to the effect of β, an observation of Figs. 10b, 10e, 11b and 11e shows that the effect of the scattering albedo ω on $\Theta(0.5, \eta_y)$ distributions is less pronounced, and the medium temperature $\Theta(0.5, \eta_y)$ decreases with an increase in ω. With an increase in ω, more radiation is scattered away, and as a result, the effect of radiation goes down, which causes a reduction in the temperature of the medium.

The effect of the conduction-radiation parameter N on $\Theta(0.5, \eta_y)$ for the four heated regions are shown in Figs. 10c, 10f, 11c and 11f. The effect of N on $\Theta(0.5, \eta_y)$ is much more pronounced than any other radiative parameters. Radiation being a non-linear process, when it is dominant $(N = 0.01)$, it causes non-linearity in the temperature profile. With an increase in N, relative contribution of conduction goes up, and the temperature profile approaches that of the pure conduction case.

4. Conclusions

This article is protected by copyright. All rights reserved.

Author Manuscript

Radiation and combined mode conduction-radiation heat transfer in a 2-D discretely heated square enclosure containing absorbing, emitting and scattering medium were analyzed. Problems were analyzed for four different discrete heated regions on the south boundary. In the problem pertaining to the radiative equilibrium, the discrete heated region was the radiation source. In the combined mode conduction-radiation problem, temperatures of the unheated regions on the south boundary and other three boundaries were 0.1 times the temperature of the discrete heated region. In the case of radiative equilibrium, distributions of radiative heat flux on the south boundary were analyzed for different values of extinction coefficient. In the combined mode problem, for the four discrete heated regions, effects of extinction coefficient, scattering albedo, conduction-radiation parameter and emissivity of the south boundary were analyzed on distributions of SS conduction, radiation and total heat fluxes along the south boundary. Effects of these parameters were also analyzed on the SS centerline temperature distributions. In the combined mode problem, with volumetric radiative information needed in the energy equation obtained from the DOM, the CDOM and the FVM, the energy equation was solved using the FDM. Including the radiative equilibrium case, in all cases, results from the three methods were in excellent agreement.

References

[1] R. Porter, F. Liu, M. Pourkashanian, A. Williams, D. Smith, Evaluation of solution methods for radiative heat transfer in gaseous oxy-fuel combustion environments, J. Quant. Spectrosc. Radiat. Transfer 111 (2010) 2084-2094.

[2] S. K. Jena, S. K. Mahapatra, Numerical modeling of interaction between surface radiation and natural convection of atmospheric aerosol in presence of transverse magnetic field, Appl. Math. Modell, 37 (2013) 527-539.

[3] V. A. Petrov, Combined radiation and conduction heat transfer in high temperature fiber thermal insulation, Int. J. Heat Mass Transfer 40 (1997) 2241-2247.

[4] C. Jang, J. Kim, T.H. Song, Combined heat transfer of radiation and conduction in stacked radiation shields for vacuum insulation panels, Energy Build. 43 (2011) 3343-3352.

[5] A. Kaemmerlen, F. Asllanaj, H. Sallée, D. Baillis, G. Jeandel, Transient modeling of combined conduction and radiation in wood fibre insulation and comparison with experimental data, Int. J. Therm. Sci. 49 (2010) 2169-2176.

[6] T.K. Kayal, M. Chakravarty, Combustion of suspended fine solid fuel in air inside inert porous medium: A heat transfer analysis, Int. J. Heat Mass Transfer 50 (2007) 3359-3365.

[7] V. Vandadi, C. Park, M. Kaviany, Superadiabatic radiant porous burner with preheater and radiation corridors, Int. J. Heat Mass Transfer 64 (2013) 680-688.

[8] C.-A. Wang, H. Sadat, V. L. Dez, Meshless method for solving multidimensional radiative transfer in graded index medium, Appl. Math. Modell, 36 (2012) 5309-5319.

This article is protected by copyright. All rights reserved.

Author Manuscript

[9] J. Okajima, S. Maruyama, H. Takeda, A. Komiya, Dimensionless solutions and general characteristics of bioheat transfer during thermal therapy, J. Therm. Biol 34 (2009) 377-384.

[10] R. Muthukumaran, S.C. Mishra, Transient response of a planar participating medium subjected to a train of short-pulse radiation, Int. J. Heat Mass Transfer 51 (2008) 2418-2432.

[11] M. Jaunich, S. Raje, K. Kim, K. Mitra, Z. Guo, Bio-heat transfer analysis during short pulse laser irradiation of tissues, Int. J. Heat Mass Transfer 51 (2008) 5511-5521.

[12] M.F. Modest, Radiative Heat Transfer, third ed., Academic press, New York, 2013.

[13] H. Ebrahimi, A. Zamaniyan, J.S.S. Mohammadzadeh, A.A. Khalili, Zonal modeling of radiative heat transfer in industrial furnaces using simplified model for exchange area calculation, Appl. Math. Modell, 37(2013) 8004-8015.

[14] R.M. Saldanha da Gama, On the conduction/radiation heat transfer problem in a body with wavelength-dependent properties, Appl. Math. Modell, 28 (2004) 795-816.

[15] K.F. Evans, The spherical harmonics discrete ordinate method for three-dimensional atmospheric radiative transfer, J. Atmos. Sci. 55 (1998) 429-446.

[16] E.W. Larsen, G. Thömmes, A. Klar, M. Seaïd, T. Götz, Simplified PN approximations to the equations of radiative heat transfer and applications, J. Comput. Phys. 183 (2002) 652-675.

[17] S. Chandrasekhar, Radiative Transfer, Dover Publications, New York, 1960.

[18] W.A. Fiveland, Discrete-ordinates solution of the radiative transport equation for rectangular enclosures, J. Heat Transfer 106 (1984) 699–706.

[19] J. S. Truelove. Three-dimensional radiation in absorbing-emitting-scattering media using the discrete-ordinates approximation. J. Quant. Spectros. Radiat. Transfer 39 (1988) 27-31.

[20] N. Selçuk, N. Kayakol, Evaluation of discrete ordinates method for radiative transfer in rectangular furnaces, Int. J. Heat Mass Transfer 40 (1997) 213-222.

[21] D. Balsara, Fast and accurate discrete ordinates methods for multidimensional radiative transfer. J. Quant. Spectros. Radiat. Transfer 69 (2001) 671-707.

[22] R. Koch, R. Becker. Evaluation of quadrature schemes for the discrete ordinates method. J. Quant. Spectros. Radiat. Transfer 84 (2004) 423-435.

[23] L.H. Liu, L.M. Ruan, H.P. Tan, On the discrete ordinates method for radiative heat transfer in anisotropically scattering media, Int. J. Heat Mass Transfer 45 (2002) 3259-326.

[24] B. Mondal, S.C. Mishra, Application of the lattice Boltzmann method and discrete ordinate method for solving transient conduction and radiation heat transfer problems, Numer. Heat Transfer A 52 (2007) 757-777.

This article is protected by copyright. All rights reserved.

Author Manuscript

[25] P.J Coelho, The role of ray effects and false scattering on the accuracy of the standard and modified discrete ordinates methods, J. Quant. Spectrosc. Radiat. Transfer 73 (2002) 231-238.

[26] H.S. Li, Reduction of false scattering in arbitrarily specified discrete directions of the discrete ordinates method, J. Quant. Spectrosc. Radiat. Transfer 86 (2004) 215-222.

[27] N.G. Shah, New method of computation of radiation heat transfer combustion chambers, PhD thesis, Imperial College, University of London, England, 1979.

[28] P.S. Cumber, M. Fairweather, Evaluation of flame emission models combined with the discrete transfer method for combustion system simulation, Int. J. Heat Mass Transfer 48 (2005) 5221–5239.

[29] N.A. Krishna, S.C. Mishra, Discrete transfer method applied to radiative transfer in a variable refractive index semitransparent medium, J. Quant. Spectrosc. Radiat. Transfer 102 (2006) 432-44.

[30] G.D. Raithby, E.H. Chui, A finite volume method for predicting radiant heat transfer in enclosures with participating media, J. Heat Transfer 112 (1990) 415–423.

[31] J.C. Chai, S.V. Patankar, Finite volume method for radiation heat transfer, Adv. Numer. Heat Transfer 2 (2000) 110–135.

[32] J.Y. Murthy, S.R. Mathur, A finite-volume scheme for radiative heat transfer in semitransparent media, Numer. Heat Transfer B 37 (2000) 25-43.

[33] S.C. Mishra, N.C. Behera, A.K. Garg, A. Mishra, Solidification of a 2-D semitransparent medium using the lattice Boltzmann method and the finite volume method, Int. J. Heat Mass Transfer 51 (2008) 4447-4460.

[34] B. Mondal, S.C. Mishra, The lattice Boltzmann method and the finite volume method applied to conduction-radiation problems with heat flux boundary conditions, Int. J. Numer. Methods Eng. 78 (2009) 172-195.

[35] H.C. Zhang, H.P. Tan, Evaluation of numerical scattering in finite volume method for solving radiative transfer equation by a central laser incidence model, J. Quant. Spectrosc. Radiat. Transfer 110 (2009) 1965-1977

[36] S.C. Mishra, H. Sahai, Analyses of non-Fourier conduction and radiation in a cylindrical medium using lattice Boltzmann method and finite volume method, Int. J. Heat Mass Transfer 61 (2013) 41-45.

[37] S.C. Mishra, H.K. Roy, N. Misra, Discrete ordinate method with a new and a simple quadrature scheme, J. Quant. Spectrosc. Radiant. Transfer 101 (2006) 249-262.

Author Manuscript

This article is protected by copyright. All rights reserved.

[38] S. C. Mishra, P. Chug, P. Kumar, K. Mitra, Development and comparison of the DTM, the DOM and the FVM formulations for the short-pulse laser transport through a participating medium, Int. J. Heat Mass Transfer 49 (2006) 1820-1832.

[39] S.C. Mishra, C. H. Krishna, Analysis of radiative transport in a cylindrical enclosure - an application of the modified discrete ordinate method, J. Quant. Spectrosc. Radiant. Transfer. 112 (2011) 1065-1081.

[40] S.C. Mishra, C. H. Krishna, M.Y. Kim, Lattice Boltzmann method and modified discrete ordinate method applied to radiative transport in a spherical medium with and without conduction, Numer. Heat Transfer A 58 (2010) 852-881.

[41] S.C. Mishra, C. H. Krishna, M.Y. Kim, Analysis of conduction and radiation heat transfer in a 2-D cylindrical medium using the modified discrete ordinate method and the lattice Boltzmann method, Numer. Heat Transfer A 60 (2011) 254-287.

[42] S.C. Mishra, P. Talukdar, D. Trimis, F. Durst, Computational efficiency improvements of the radiative transfer problems with or without conduction - a comparison of the collapsed dimension method and the discrete transfer method, Int. J. Heat Mass Transfer 46 (2002) 3083-3095.

Author Manuscript

Control volumes $N_x \times N_y$	Rays $M_\theta \times M_\phi$	Radiative heat flux							
		CDOM		DOM		FVM		DTM	
		Location, η_x		Location, η_x		Location, η_x		Location, η_x	
		0.25	0.5	0.25	0.5	0.25	0.5	0.25	0.5
10×10	6×8	0.7830	0.7642	0.7736	0.7523	0.7779	0.7571	0.7797	0.7576
20×20		0.7825	0.7633	0.7734	0.7517	0.777	0.7505		
30×30		0.7823	0.7631	0.7728	0.7515	0.7771	0.7561		
40×40		0.7824	0.7632	0.7728	0.7515	0.7771	0.7561		

This article is protected by copyright. All rights reserved.

30×30	2×4	0.8804	0.8636	0.7491	0.7187	0.7491	0.7187	0.7797	0.7576
	4×6	0.8238	0.8064	0.7677	0.7457	0.7677	0.7457		
	6×8	0.7823	0.7631	0.7728	0.7515	0.7771	0.7561		

Table 1: Comparison of radiative heat flux at locations η_x = 0.25 and 0.5 on south boundary for different numbers of control volumes and rays; $\beta = 1.0$.

Author Manuscript

This article is protected by copyright. All rights reserved.

List of Figures

Figure 1: (a) Schematic of the 2-D square enclosure marching directions of intensities from the four quadrants, and (b) coordinate system used.

Figure 2: Variation of non-dimensional heat flux $\Psi(\eta_x, 0.0)$ with non-dimensional distance η_x for extinction coefficient $\beta = 0.1$, 1.0 and 3.0 for heating region (a) $0.0 \le \eta_x \le 1.0$, (b) $0.33 \le \eta_x \le 0.66$, (c) $0 \le \eta_x \le 0.33$, (d) $0 \le \eta_x \le 0.66$ and (e) $0 \le \eta_x \le 0.33$ and $0.66 \le \eta_x \le 1.0$.

Figure 3: Variation of conduction heat flux Ψ_C, radiation heat flux Ψ_R and total heat flux Ψ_T with distance η_x for (a)-(c) heating region $0.0 \le \eta_x \le 1.0$ for extinction coefficient (a) $\beta = 0.1$, (b) $\beta =$ 0.1 and (c) $\beta = 5.0$; (d)-(f) for heating region $0.33 \le \eta_x \le 0.66$ for (d) $\beta = 0.1$, (e) $\beta = 0.1$ and (f) $\beta = 5.0$; $\omega = 0.5, N = 0.1, \varepsilon = 1.0$.

Figure 4: Variation of conduction heat flux Ψ_C, radiation heat flux Ψ_R and total heat flux Ψ_T with distance η_x for (a)-(c) heating region $0.0 \le \eta_x \le 0.33$ for extinction coefficient (a) $\beta = 0.1$, (b) $\beta =$ 0.1 and (c) $\beta = 5.0$; (d)-(f) for heating region $0.0 \le \eta_x \le 0.66$ for (d) $\beta = 0.1$, (e) $\beta = 0.1$ and (f) $\beta = 5.0$; $\omega = 0.5, N = 0.1, \varepsilon = 1.0$.

Figure 5: Variation of conduction heat flux Ψ_C, radiation heat flux Ψ_R and total heat flux Ψ_T with distance η_x for (a)-(c) heating region $0.0 \le \eta_x \le 1.0$ for scattering albedo (a) $\omega = 0.0$, (b) $\omega = 0.5$ and (c) $\omega = 0.8$; (d)-(f) for heating region $0.33 \le \eta_x \le 0.66$ for (d) $\omega = 0.0$, (e) $\omega = 0.5$ and (f) $\omega =$ 0.8; $\beta = 1.0, N = 0.1, \varepsilon = 1.0$.

Figure 6: Variation of conduction heat flux Ψ_C, radiation heat flux Ψ_R and total heat flux Ψ_T with distance η_x for (a)-(c) heating region $0.0 \le \eta_x \le 0.33$ for scattering albedo (a) $\omega = 0.0$, (b) $\omega = 0.5$ and (c) $\omega = 0.8$; (d)-(f) for heating region $0.0 \le \eta_x \le 0.66$ for (d) $\omega = 0.0$, (e) $\omega = 0.5$ and (f) $\omega =$ 0.8; $\beta = 1.0, N = 0.1, \varepsilon = 1.0$.

Figure 7: Variation of conduction heat flux Ψ_C, radiation heat flux Ψ_R and total heat flux Ψ_T with distance η_x for (a)-(c) heating region $0.0 \le \eta_x \le 1.0$ for conduction-radiation parameter (a) $N =$ 0.01, (b) $N = 0.1$ and (c) $N = 1.0$; (d)-(f) for heating region $0.33 \le \eta_x \le 0.66$ for (d) $N = 0.01$, (e) $N = 0.1$ and (f) $N = 1.0$; $\beta = 1.0, \omega = 0.0, \varepsilon = 1.0$.

Figure 8: Variation of conduction heat flux Ψ_C, radiation heat flux Ψ_R and total heat flux Ψ_T with distance η_x for (a)-(c) heating region $0.0 \le \eta_x \le 0.33$ for conduction-radiation parameter (a) $N =$

This article is protected by copyright. All rights reserved.

Author Manuscript

0.01, (b) $N = 0.1$ and (c) $N = 1.0$; (d)-(f) for heating region $0.0 \le \eta_x \le 0.66$ for (d) $N = 0.01$, (e) $N = 0.1$ and (f) $N = 1.0$; $\beta = 1.0, \omega = 0.0, \varepsilon = 1.0.$

Figure 9: Variation of conduction heat flux Ψ_C, radiation heat flux Ψ_R and total heat flux Ψ_T with distance η_x for (a)-(c) heating region $0.0 \le \eta_x \le 1.0$ for south wall emissivity (a) $\varepsilon_S = 0.2$, (b) $\varepsilon_S = 0.6$ and (c) $\varepsilon_S = 1.0$; (d)-(f) for heating region $0.0 \le \eta_x \le 0.33$ for (d) $\varepsilon_S = 0.2$, (e) $\varepsilon_S = 0.6$ and (f) $\varepsilon_S = 1.0$; $\beta = 0.1, \omega = 0.5, N = 0.1.$

Figure 10: Variation of centerline $(\eta_x = 0.5, \eta_y)$ temperature Θ for heating region $0.0 \le \eta_x \le 1.0$ for (a) $\beta = 0.1$, 1.0 and 5.0, (b) $\omega = 0.0$, 0.5 and 0.8, (c) $N = 0.01$, 0.1 and 1.0; for heating region $0.33 \le \eta_x \le 0.66$ for (d) $\beta = 0.1$, 1.0 and 5.0, (e) $\omega = 0.0$, 0.5 and 0.8, (f) $N = 0.01$, 0.1 and 1.0.

Figure 11: Variation of centerline $(\eta_x = 0.5, \eta_y)$ temperature Θ for heating region $0.0 \le \eta_x \le 0.33$ for (a) $\beta = 0.1$, 1.0 and 5.0, (b) $\omega = 0.0$, 0.5 and 0.8, (c) $N = 0.01$, 0.1 and 1.0; for heating region $0.0 \le \eta_x \le 0.66$ for (d) $\beta = 0.1$, 1.0 and 5.0, (e) $\omega = 0.0$, 0.5 and 0.8, (f) $N = 0.01$, 0.1 and 1.0.

Author Manuscript

This article is protected by copyright. All rights reserved.

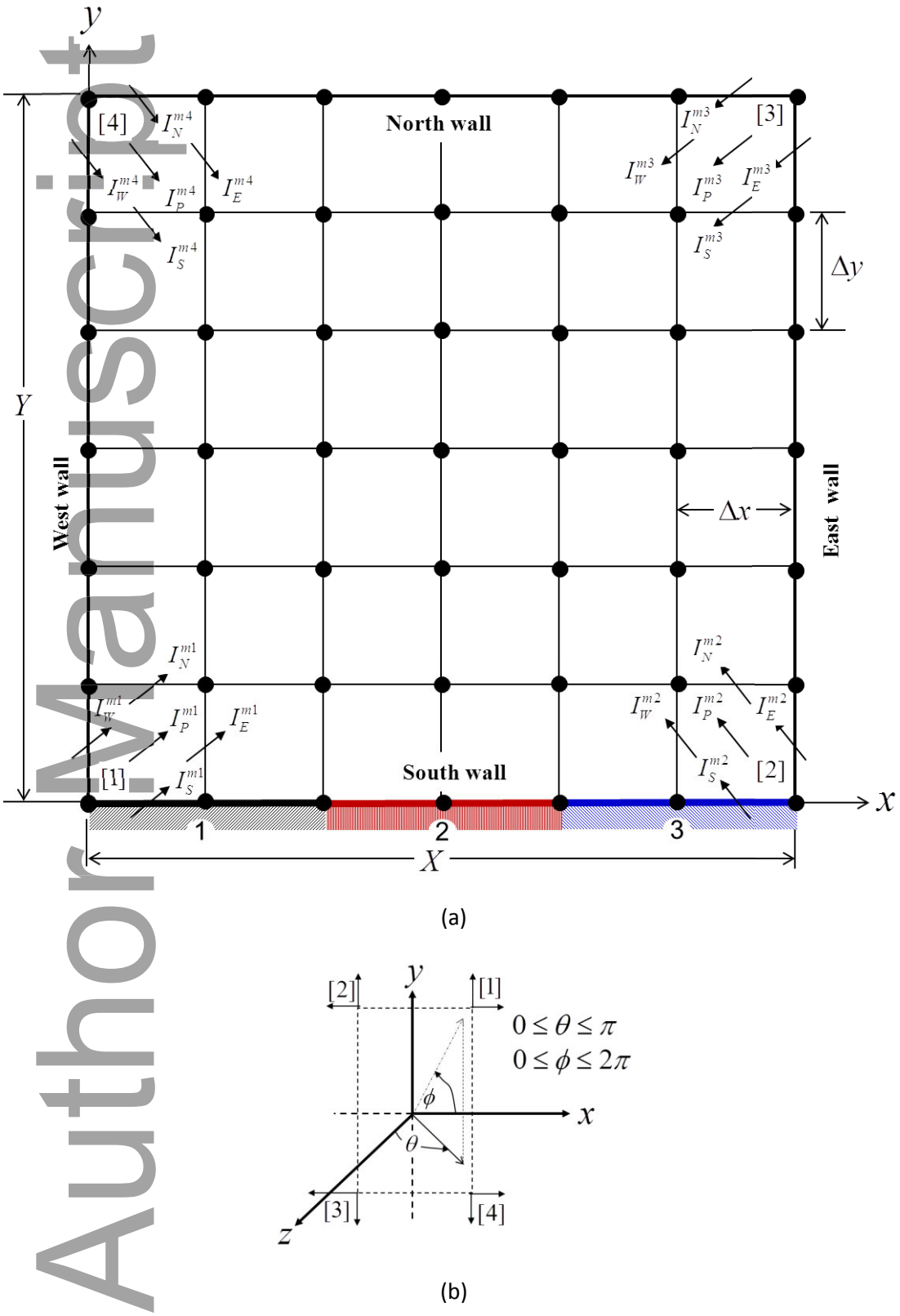
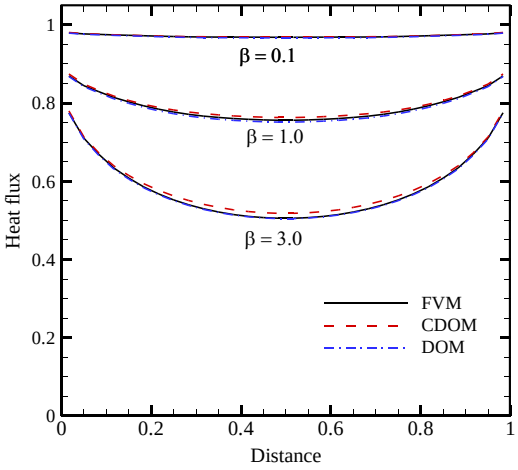


Figure 1: (a) Schematic of the 2-D square enclosure marching directions of intensities from the

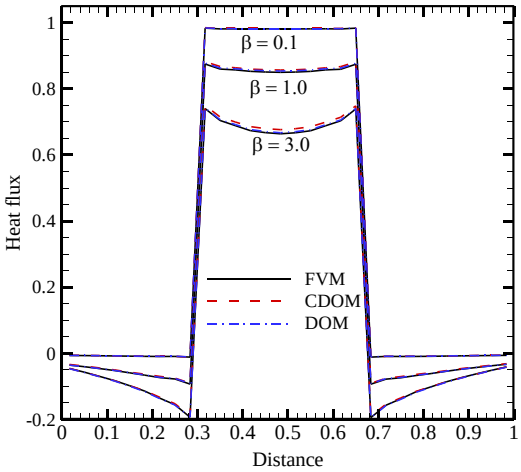
Author Manuscript

This article is protected by copyright. All rights reserved.

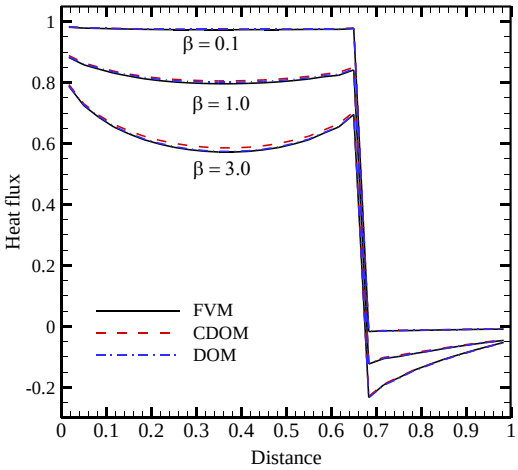
four quadrants, and (b) coordinate system used.



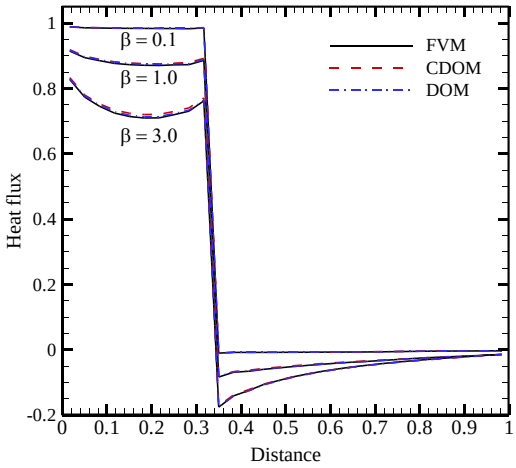
(a)



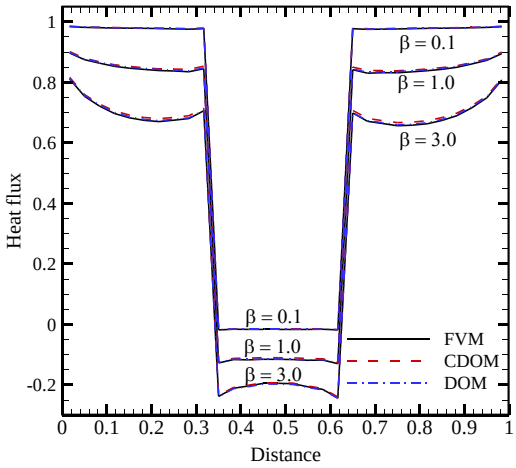
(b)



(d)



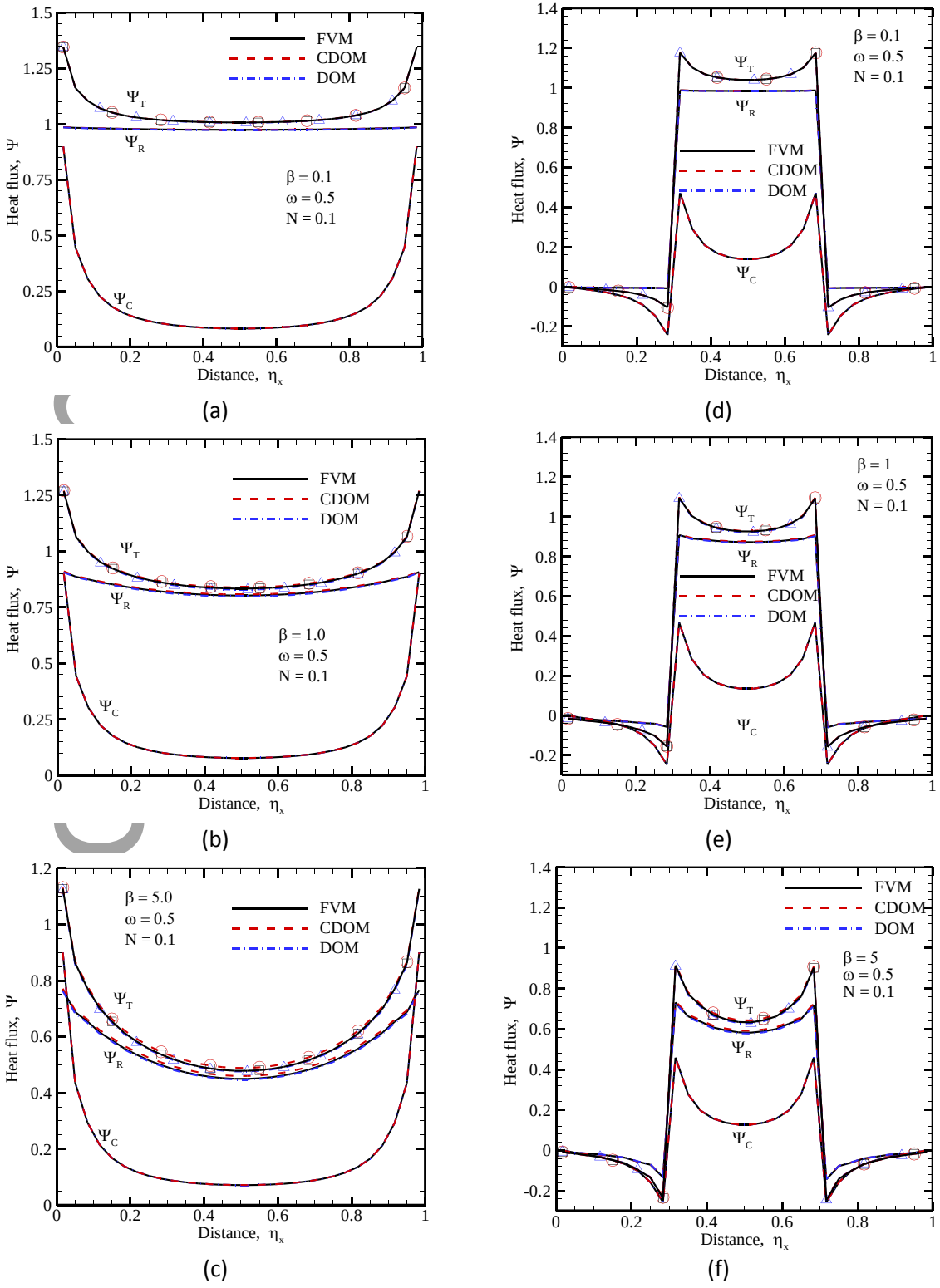
(c)



(e)

This article is protected by copyright. All rights reserved.

Figure 2: Variation of non-dimensional heat flux $\Psi(\eta_x, 0.0)$ with non-dimensional distance η_x for extinction coefficient $\beta = 0.1$, 1.0 and 3.0 for heating region (a) $0.0 \le \eta_x \le 1.0$, (b) $0.33 \le \eta_x \le 0.66$, (c) $0 \le \eta_x \le 0.33$, (d) $0 \le \eta_x \le 0.66$ and (e) $0 \le \eta_x \le 0.33$ and $0.66 \le \eta_x \le 1.0$.



This article is protected by copyright. All rights reserved.

Figure 3: Variation of conduction heat flux Ψ_C, radiation heat flux Ψ_R and total heat flux Ψ_T with distance η_x for (a)-(c) heating region $0.0 \le \eta_x \le 1.0$ for extinction coefficient (a) $\beta = 0.1$, (b) $\beta = 0.1$ and (c) $\beta = 5.0$; (d)-(f) for heating region $0.33 \le \eta_x \le 0.66$ for (d) $\beta = 0.1$, (e) $\beta = 0.1$ and (f) $\beta = 5.0$; $\omega = 0.5, N = 0.1, \varepsilon = 1.0$.

Author Manuscript

This article is protected by copyright. All rights reserved.

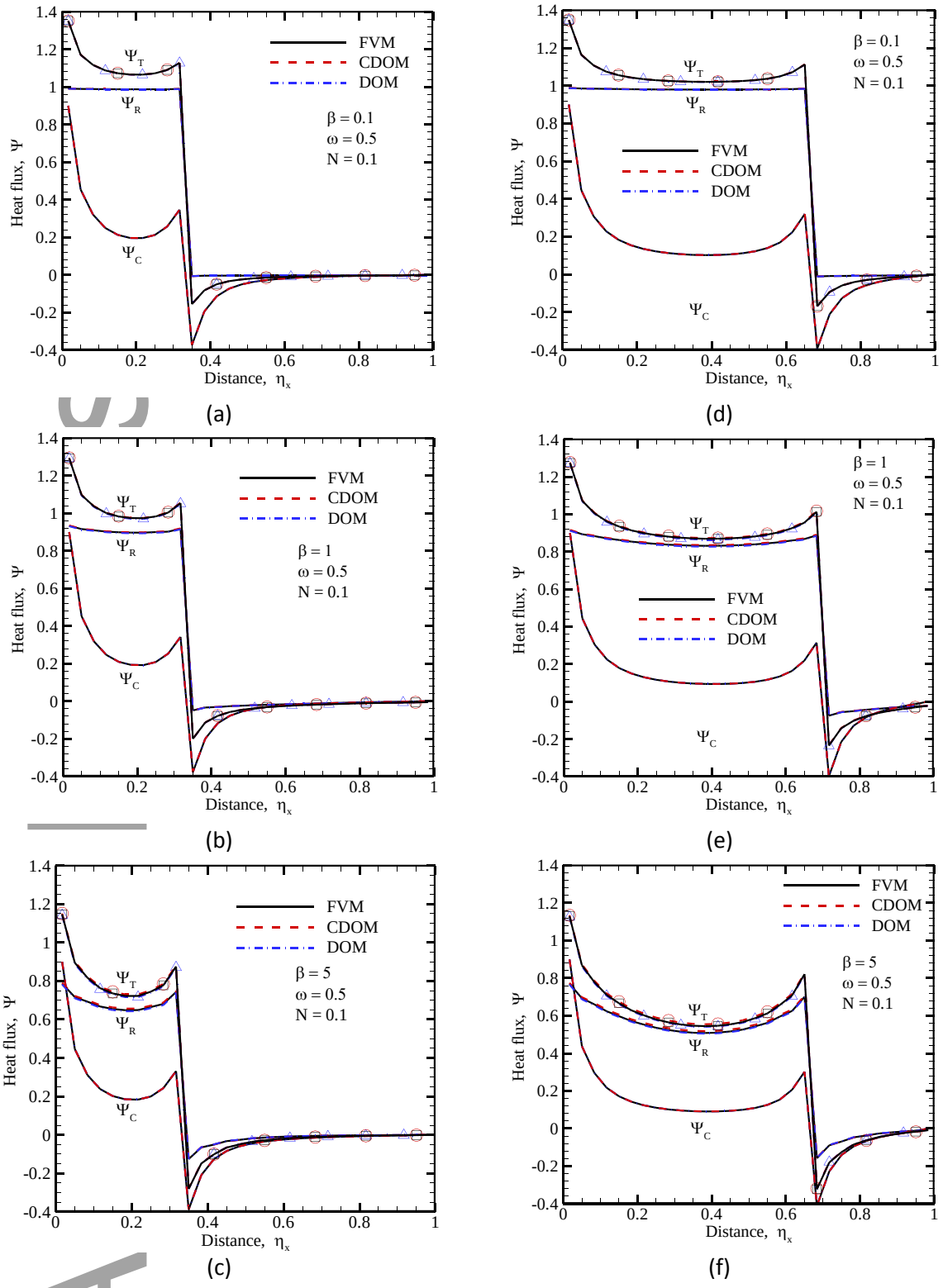


Figure 4: Variation of conduction heat flux Ψ_C, radiation heat flux Ψ_R and total heat flux Ψ_T with distance η_x for (a)-(c) heating region $0.0 \le \eta_x \le 0.33$ for extinction coefficient (a) $\beta = 0.1$, (b) $\beta = 0.1$ and (c) $\beta = 5.0$; (d)-(f) for heating region $0.0 \le \eta_x \le 0.66$ for (d) $\beta = 0.1$, (e) $\beta = 0.1$ and (f) $\beta = 5.0$; $\omega = 0.5, N = 0.1, \varepsilon = 1.0$.

This article is protected by copyright. All rights reserved.

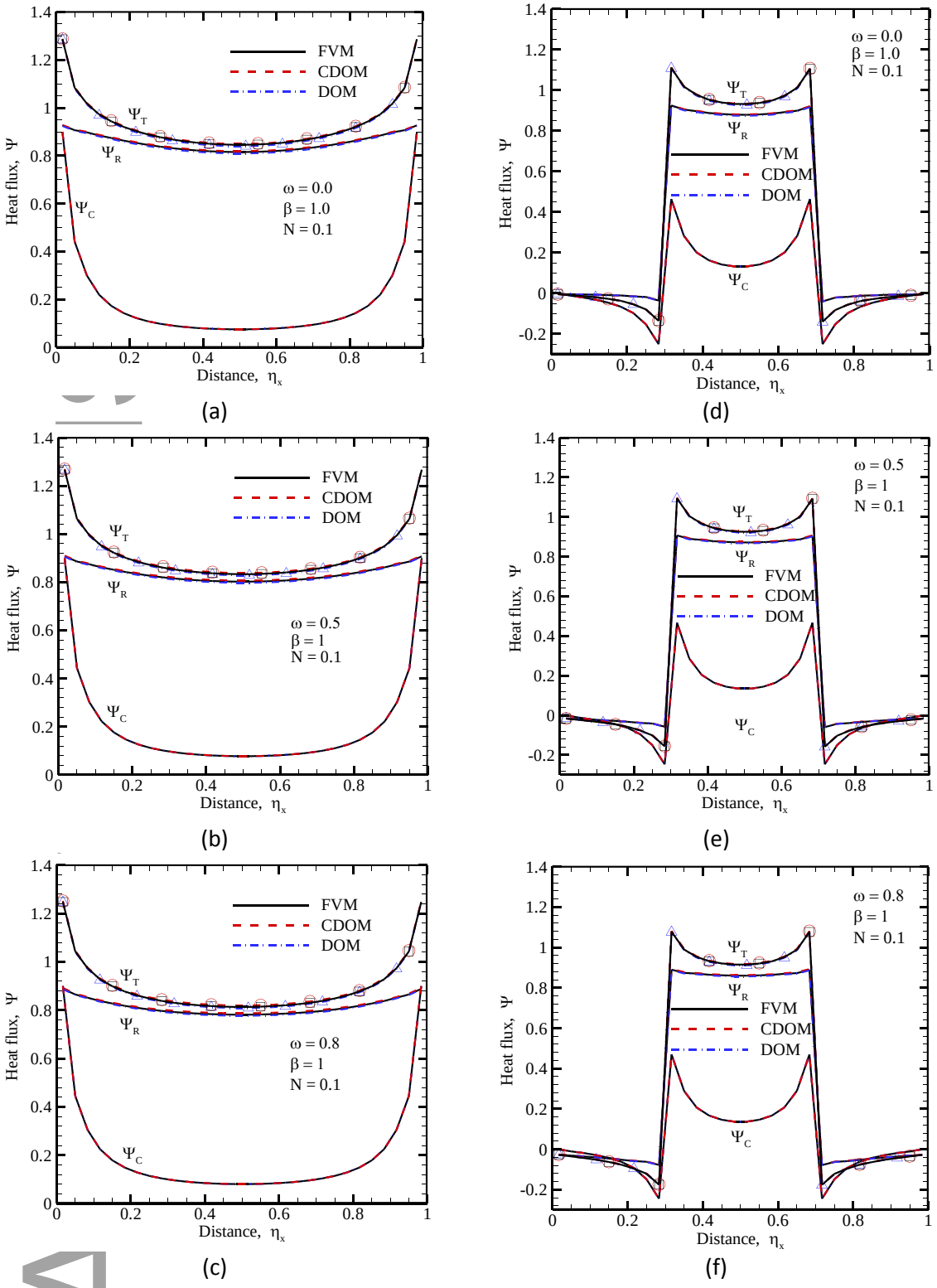
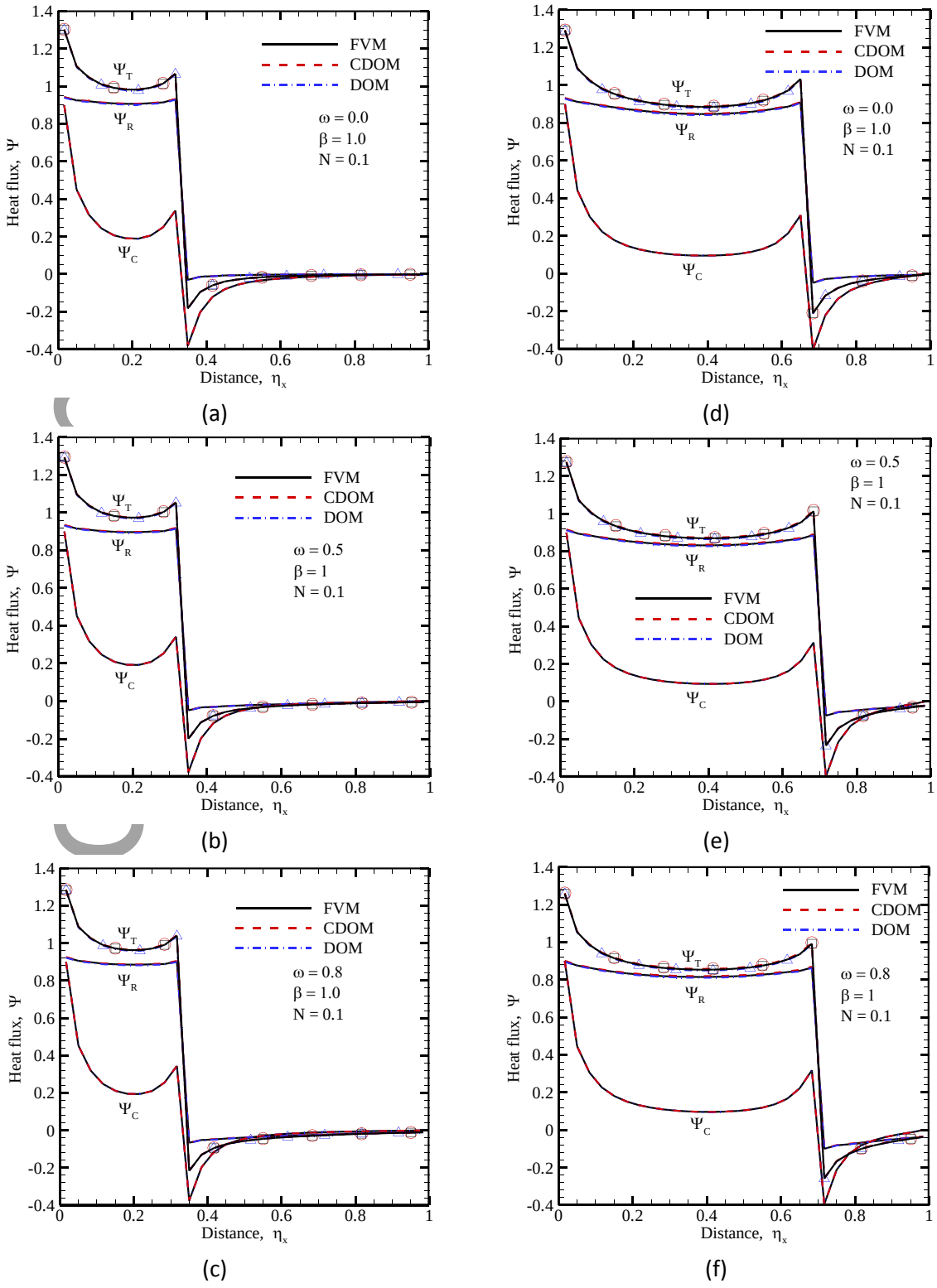


Figure 5: Variation of conduction heat flux Ψ_C, radiation heat flux Ψ_R and total heat flux Ψ_T with distance η_x for (a)-(c) heating region $0.0 \le \eta_x \le 1.0$ for scattering albedo (a) $\omega = 0.0$, (b) $\omega = 0.5$ and (c) $\omega = 0.8$; (d)-(f) for heating region $0.33 \le \eta_x \le 0.66$ for (d) $\omega = 0.0$, (e) $\omega = 0.5$

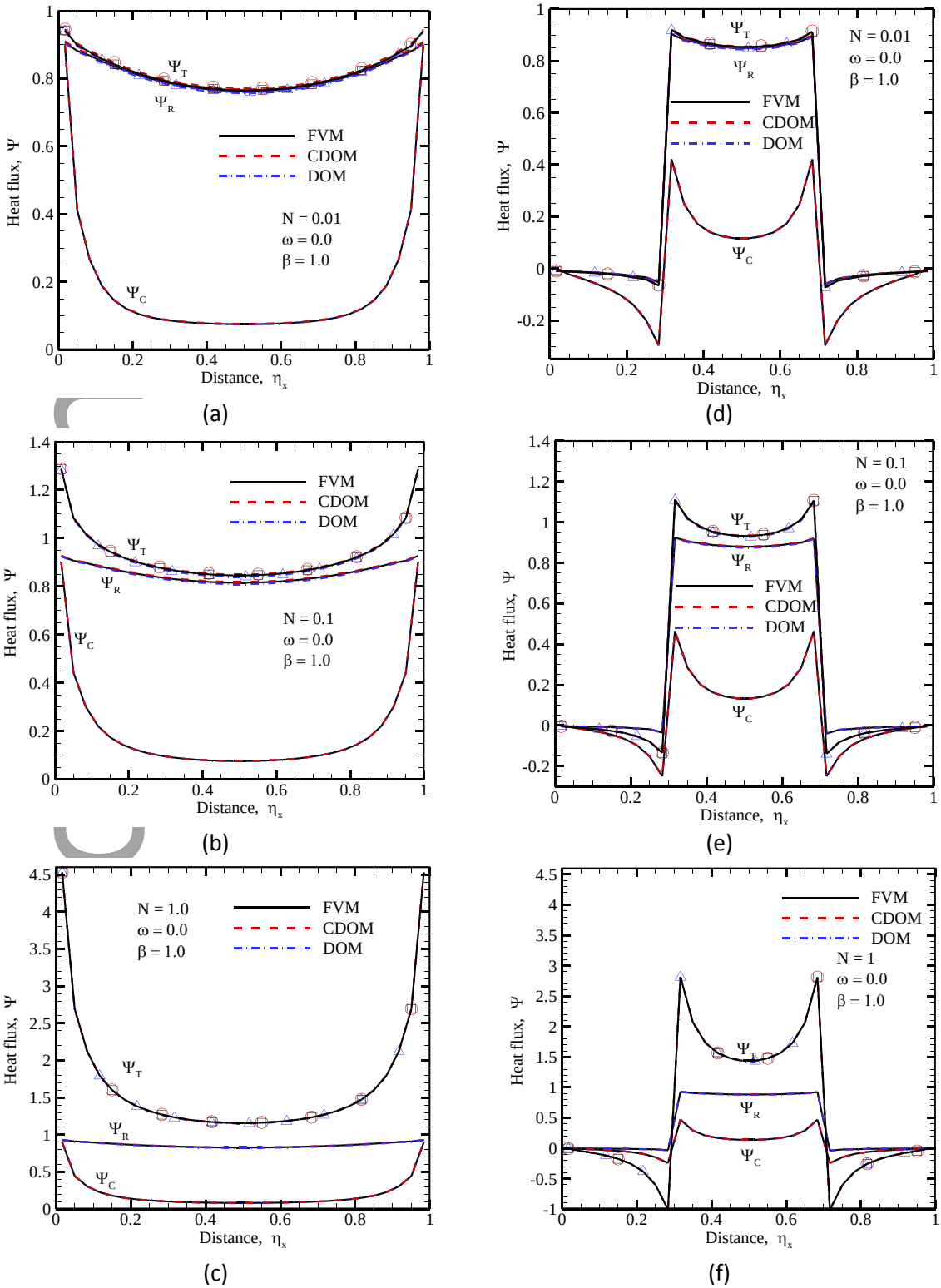
This article is protected by copyright. All rights reserved.

and (f) $\omega = 0.8;\ \beta = 1.0, N = 0.1, \varepsilon = 1.0.$



This article is protected by copyright. All rights reserved.

Figure 6: Variation of conduction heat flux Ψ_C, radiation heat flux Ψ_R and total heat flux Ψ_T with distance η_x for (a)-(c) heating region $0.0 \le \eta_x \le 0.33$ for scattering albedo (a) $\omega = 0.0$, (b) $\omega = 0.5$ and (c) $\omega = 0.8$; (d)-(f) for heating region $0.0 \le \eta_x \le 0.66$ for (d) $\omega = 0.0$, (e) $\omega = 0.5$ and (f) $\omega = 0.8$; $\beta = 1.0, N = 0.1, \varepsilon = 1.0$.



This article is protected by copyright. All rights reserved.

Figure 7: Variation of conduction heat flux Ψ_{C}, radiation heat flux Ψ_{R} and total heat flux Ψ_{T} with distance η_x for (a)-(c) heating region $0.0 \le \eta_x \le 1.0$ for conduction-radiation parameter (a) $N = 0.01$, (b) $N = 0.1$ and (c) $N = 1.0$; (d)-(f) for heating region $0.33 \le \eta_x \le 0.66$ for (d) $N = 0.01$, (e) $N = 0.1$ and (f) $N = 1.0$; $\beta = 1.0, \omega = 0.0, \varepsilon = 1.0$.

Author Manuscript

This article is protected by copyright. All rights reserved.

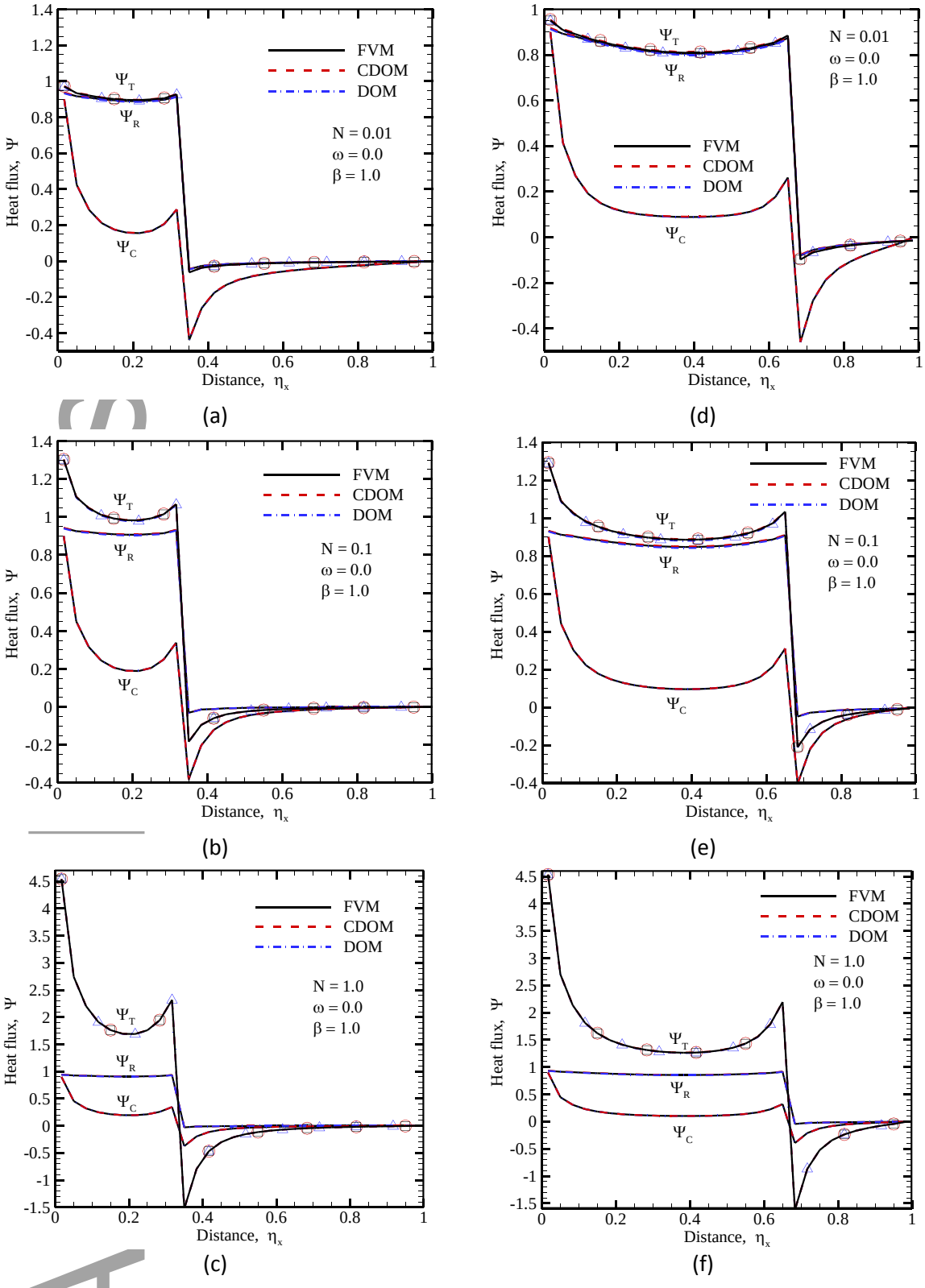
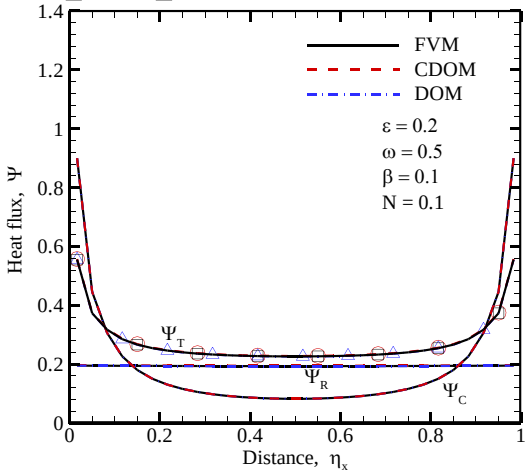
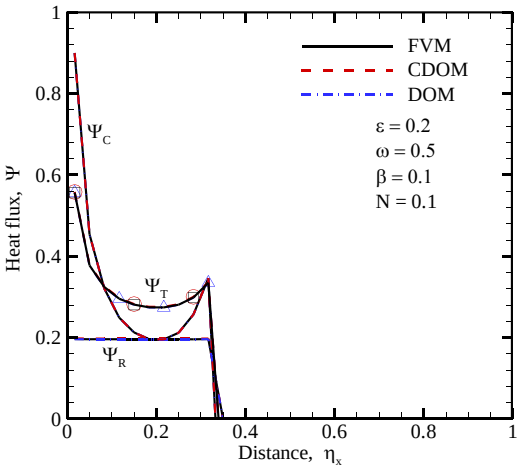


Figure 8: Variation of conduction heat flux Ψ_C, radiation heat flux Ψ_R and total heat flux Ψ_T with distance η_x for (a)-(c) heating region $0.0 \le \eta_x \le 0.33$ for conduction-radiation parameter (a) $N = 0.01$, (b) $N = 0.1$ and (c) $N = 1.0$; (d)-(f) for heating region $0.0 \le \eta_x \le 0.66$ for (d) $N = 0.01$, (e) $N = 0.1$ and (f) $N = 1.0$; $\beta = 1.0, \omega = 0.0, \varepsilon = 1.0$.

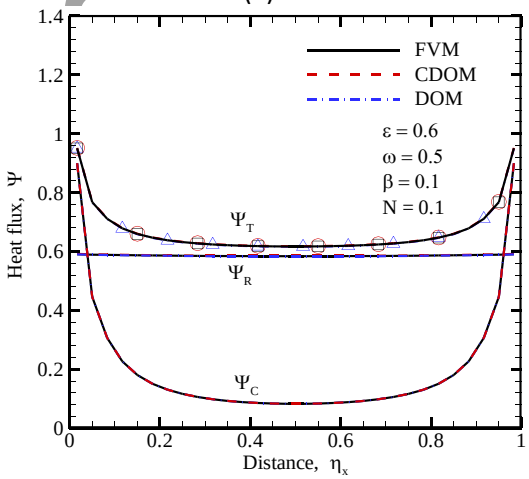
This article is protected by copyright. All rights reserved.



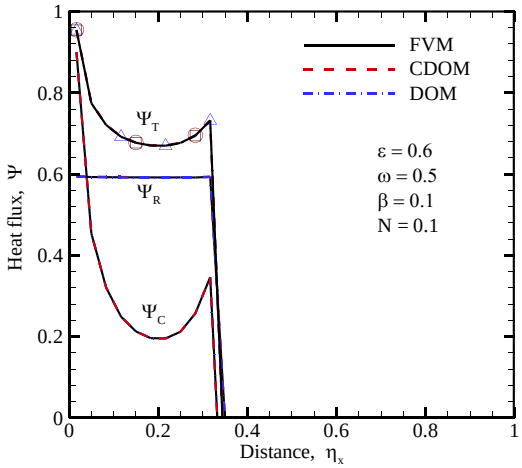
(a)



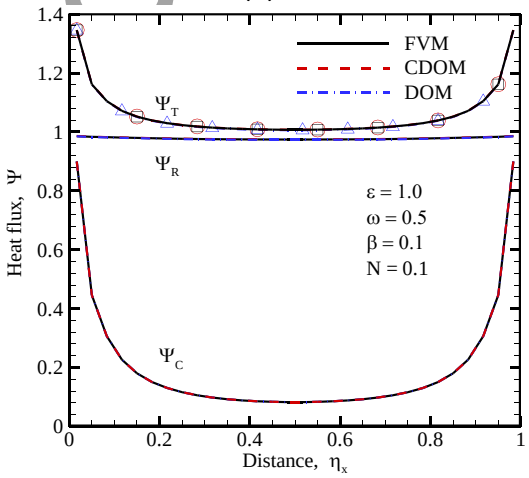
(d)



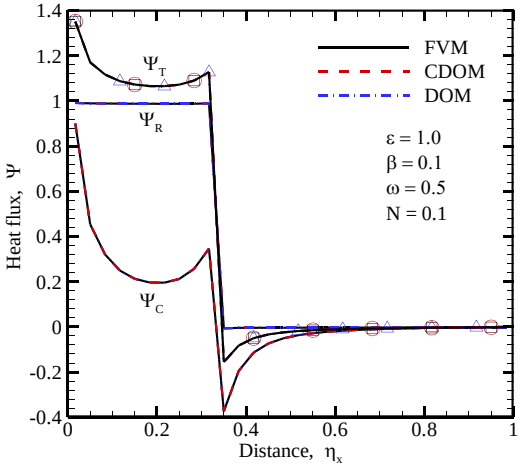
(b)



(e)



(c)



(f)

This article is protected by copyright. All rights reserved.

Figure 9: Variation of conduction heat flux Ψ_{C}, radiation heat flux Ψ_{R} and total heat flux Ψ_{T} with distance η_x for (a)-(c) heating region $0.0 \le \eta_x \le 1.0$ for south wall emissivity (a) $\varepsilon_S = 0.2$, (b) $\varepsilon_S = 0.6$ and (c) $\varepsilon_S = 1.0$; (d)-(f) for heating region $0.0 \le \eta_x \le 0.33$ for (d) $\varepsilon_S = 0.2$, (e) $\varepsilon_S = 0.6$ and (f) $\varepsilon_S = 1.0$; $\beta = 0.1, \omega = 0.5, N = 0.1$.

Author Manuscript

This article is protected by copyright. All rights reserved.

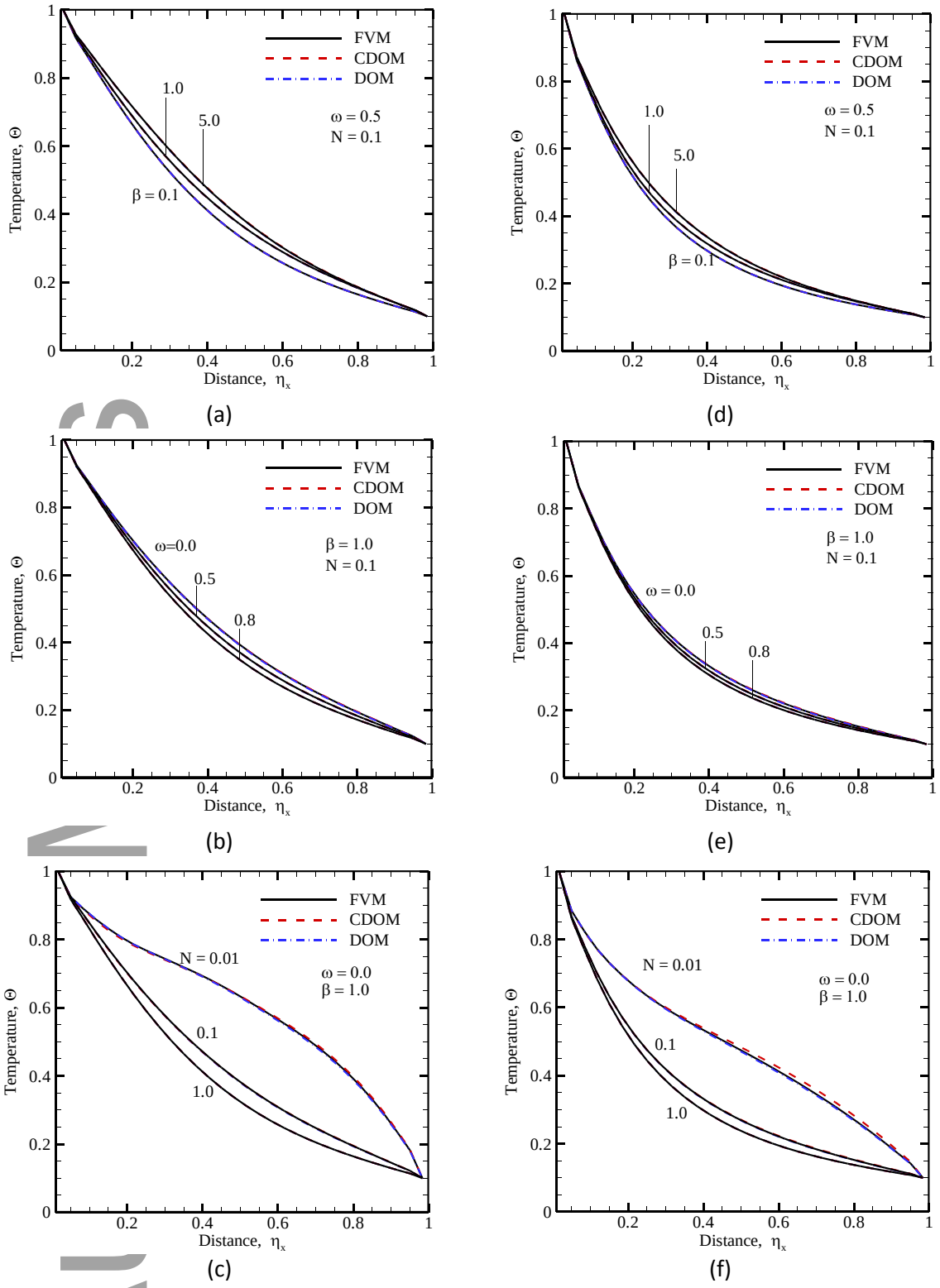


Figure 10: Variation of centerline $(\eta_x = 0.5, \eta_y)$ temperature Θ for heating region $0.0 \le \eta_x \le 1.0$ for (a) $\beta = 0.1$, 1.0 and 5.0, (b) $\omega = 0.0$, 0.5 and 0.8, (c) $N = 0.01$, 0.1 and 1.0; for heating region $0.33 \le \eta_x \le 0.66$ for (d) $\beta = 0.1$, 1.0 and 5.0, (e) $\omega = 0.0$, 0.5 and 0.8, (f) $N = 0.01$, 0.1 and 1.0.

This article is protected by copyright. All rights reserved.

Author Manuscript

This article is protected by copyright. All rights reserved.

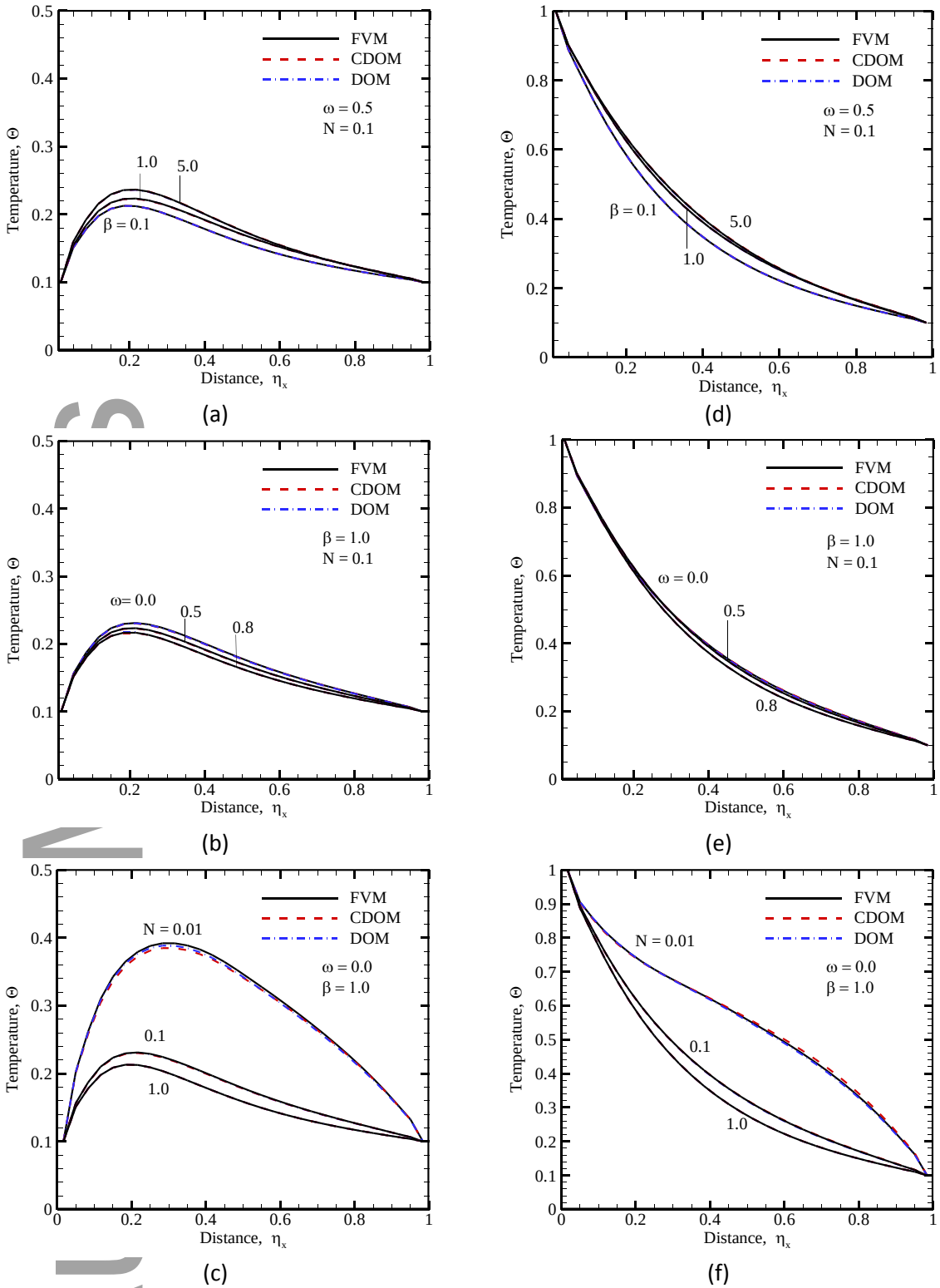


Figure 11: Variation of centerline $(\eta_x = 0.5, \eta_y)$ temperature Θ for heating region $0.0 \le \eta_x \le 0.33$ for (a) $\beta = 0.1$, 1.0 and 5.0, (b) $\omega = 0.0$, 0.5 and 0.8, (c) $N = 0.01$, 0.1 and 1.0; for heating region $0.0 \le \eta_x \le 0.66$ for (d) $\beta = 0.1$, 1.0 and 5.0, (e) $\omega = 0.0$, 0.5 and 0.8, (f) $N = 0.01$, 0.1 and 1.0.

This article is protected by copyright. All rights reserved.

Author Manuscript

This article is protected by copyright. All rights reserved.